

Effect of Process Variables on Transformation-Texture Development in Ti-6Al-4V Sheet Following Beta Heat Treatment

S.L. SEMIATIN, K.T. KINSEL, A.L. PILCHAK, and G.A. SARGENT

The effect of preheat time, prestrain, cooling rate, and concurrent deformation during cooling on the preferential selection of hcp alpha variants during the decomposition of the high-temperature, bcc beta phase in two-phase titanium alloys was established using Ti-6Al-4V sheet material. For this purpose, sheet tension samples were pre-soaked in the beta phase field for 0 or 10 minutes (to vary the beta grain size), subjected to a prestrain of 0 or 0.1, and cooled at a rate of 11 or 155 K/min (11 or 155 °C/min) under conditions comprising free ends, fixed ends, or concurrent deformation at a strain rate between $\sim 10^{-5}$ and $3 \times 10^{-4} \text{ s}^{-1}$. Electron-backscatter diffraction was used to determine the orientations of the alpha variants so formed, from which the underlying high-temperature, beta-grain microstructure and orientations were reconstructed. These measurements revealed that the parent beta texture changed due to grain growth during preheating. A comparison of the alpha- and beta-phase textures indicated that preferential variant selection was most noticeable under conditions involving a slow cooling rate especially when prestrain or concurrent straining was imposed.

DOI: 10.1007/s11661-013-1735-6

© The Minerals, Metals & Materials Society and ASM International 2013

I. INTRODUCTION

COMMERCIAL alpha/beta and near-alpha titanium alloys often exhibit a high degree of property directionality. This directionality is associated with moderate-to-strong crystallographic textures of the hcp alpha phase, which comprises a majority of the microstructure, and its limited number of slip systems. Texture can form as a result of deformation, recrystallization, transformation, or a combination of all three processes.

Titanium parts which require high strength, ductility, and resistance to fatigue crack initiation are typically processed in the two-phase (alpha + beta) field to yield a microstructure of equiaxed, primary-alpha particles in a matrix of transformed beta. The texture of the primary alpha is determined by rotations due to (1) metal flow and (2) crystallographic slip whose magnitude is a function of the strain partitioning between the (softer) beta and (harder) alpha phases.^[1,2] The texture of so-called secondary-alpha platelets which form within the bcc beta matrix during cooling following hot working in the two-phase field is usually similar to that of the primary alpha. It has been hypothesized that local stresses developed in two-phase material during cooling

(as a result of differences in coefficients of thermal expansion) tend to favor the formation of alpha variants whose orientation is similar to that of the primary alpha.^[3] Such biasing of the texture of the secondary alpha by that of the primary alpha has been modeled based on a minimum strain-energy hypothesis.^[4] In other work, it has been postulated that the anisotropic contraction of primary alpha during cooling may activate slip on selected {110} slip planes in the beta phase, thus biasing the secondary-alpha variants that are formed.^[5]

When good toughness and creep resistance are required in alpha/beta titanium components, hot-working or heat treatment in the high-temperature, singlephase beta field is usually performed. These thermomechanical processes produce a transformed microstructure of lamellar alpha in a matrix of beta. The transformation follows a classical Burgers orientation relationship^[6,7] such that the respective closed-packed planes and directions of the parent beta and product alpha phases are parallel to each other; *e.g.*, $(110)_\beta \parallel (0001)_\alpha$ and $[1\bar{1}\bar{1}]_\beta \parallel [2\bar{1}\bar{1}0]_\alpha$. Because there are six {110}-type planes and two $\langle 111 \rangle$ -type directions on each of these planes in a bcc crystal, twelve distinct alpha variants may be developed within each beta grain of a polycrystalline aggregate. If all twelve variants were to form within each beta grain, the transformation texture would be relatively weak. From observations on 2-D sections, it often appears, however, that only a small subset of the possible variants predominates within each grain, thus leading to overall textures of various strengths.

Investigations of the effect of process variables on variant selection following beta annealing have produced sometimes-conflicting results, especially for the

S.L. SEMIATIN, Senior Scientist, Materials Processing/Processing Science and A.L. PILCHAK, Materials Research Engineer, are with the AFRL/RXCM, Air Force Research Laboratory, Materials and Manufacturing Directorate, Wright-Patterson Air Force Base, OH 45433-7817. Contact e-mail: Lee.Semiatin@wpafb.af.mil K.T. KINSEL, formerly Undergraduate Student with the Wright-State University, Dayton, OH 45435, is now Graduate Student with the Department of Materials Science and Engineering, The Ohio State University, Columbus, OH 43210 G.A. SARGENT, Consultant, is with UES, Inc., 4401 Dayton-Xenia Road, Dayton, OH 45432.

Manuscript submitted November 28, 2012.

Article published online April 17, 2013

most common alpha/beta titanium alloy, Ti-6Al-4V. For example, under very slow cooling conditions (~ 1 K/min, or ~ 1 °C/min), Stanford and Bate^[8] and Obasi *et al.*^[9] have noted a strong degree of variant selection, especially for samples with a coarse beta grain size. This trend was ascribed to the preferential nucleation of certain alpha variants at the beta grain boundaries and their subsequent growth as alpha sideplates.^[10,11] At very high cooling rates typical of water quenching, strong variant selection has also been observed.^[12] By contrast, preferential variant selection was found to be minimal when *intermediate* cooling rates (~ 10 K/min, or ~ 10 °C/min) were used.^[13]

Relatively strong alpha-phase transformation textures have also been observed in Ti-6Al-4V which has been *hot worked* to effective strains between 0.4 and 1.6 in the beta field prior to cooling.^[14] For the case involving the largest strain, the selected variants tended to correlate with the beta slip systems which had been most active during the prior deformation.^[15]

The objective of the present work was to provide further insight into and clarification of the effect of process variables on variant selection in alpha/beta titanium alloys. A sheet product form was utilized in view of the increasing interest in such materials for high-temperature structural applications limited by creep in which a transformed (colony-alpha) microstructure is beneficial. The process variables investigated included soak time and prestrain prior to cooling, cooling rate, and stress/strain state during cooling.

II. MATERIALS AND PROCEDURES

A. Materials

The material used in this investigation was Ti-6Al-4V with a measured composition (in weight percent) of 6.08 aluminum, 3.89 vanadium, 0.15 oxygen, 0.19 iron, 0.008 nitrogen, 0.014 carbon, 0.0044 hydrogen, with the balance being titanium. It was received as 1.5-mm thick sheet in the hot-rolled-and-surface-ground condition. The beta-transus temperature (at which $\alpha + \beta \rightarrow \beta$) was 1268 K (995 °C).

The microstructure of the as-received sheet material consisted of primary-alpha particles and a small fraction (<10 pct.) of fine beta grains (Figure 1(a)). As characterized by $(0001)_\alpha$ (basal) pole figures, the alpha-phase texture was moderately strong; it comprised primarily a component along the transverse direction (TD) and weaker components lying along the rolling direction (RD) and a direction lying between the normal direction (ND) and RD (Figure 1b). In these and subsequent pole figures, the RD and TD are at the 12 and 9 o'clock positions, respectively, and the ND is located at the center. Furthermore, texture intensities are reported in times-random units in all cases.

By and large, the beta-phase texture of the as-received sheet, as exemplified by a $(110)_\beta$ pole figure (Figure 1(b)), was typical of a bcc rolling texture with an additional split component between the ND and RD. Although the Burgers orientation relation was eliminated by hot rolling below the beta-transus temperature, some of the

components of this texture, although weaker, mirrored those in the alpha-phase texture.

B. Experimental Procedures

To establish the effect of process variables on variant selection, dogbone-shaped tension samples (Figure 2) were electric-discharge machined (EDM'ed) along the RD of the as-received Ti-6Al-4V sheet and subjected to various types of beta-annealing-and-cooling cycles. Process variables such as cooling rate, stress state, and strain rate during cooling were chosen to mimic those that are experienced during the final heat treatment of large-scale, fracture-critical, titanium components.

For the initial, or baseline, experiments, samples were mounted in a servohydraulic mechanical-testing machine, and the reduced section, fillets, and a portion of the shoulder regions of each sample were heated using an indirect-resistance furnace. To avoid oxidation, each test specimen was enclosed in a quartz tube through which dried argon was passed. The heating cycle consisted of raising the sample temperature to 1233 K (960 °C) at a rate of ~ 160 K/min (~ 160 °C/min), holding for 3 minutes to dissolve most of the primary alpha

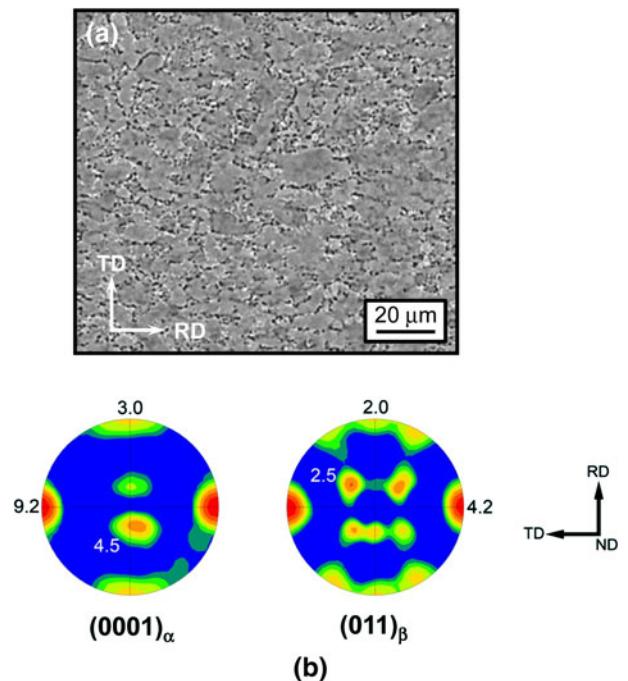


Fig. 1—Microstructure and texture of the as-received Ti-6Al-4V sheet material: (a) Backscattered-electron (BSE) image (alpha is the darker phase, and beta/transformed beta is lighter) and (b) $(0001)_\alpha$ and $(011)_\beta$ pole figures.

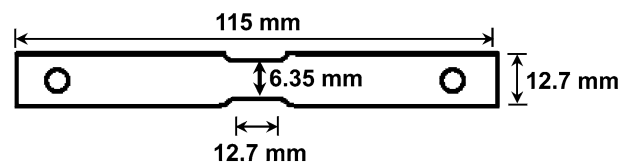


Fig. 2—Tension-sample geometry.

and to homogenize the composition of the beta phase, and then heating at a rate of 80 K/min (80 °C/min) to a temperature of $1285 \text{ K} \pm 2 \text{ K}$ ($1012 \pm 2 \text{ °C}$); *i.e.*, $\sim 15 \text{ K}$ ($\sim 15 \text{ °C}$) above the beta-transus temperature. Upon reaching the peak temperature, the sample was soaked for 0 or 10 minutes to obtain two different beta grain sizes. Following the soak period, controlled cooling at a constant rate of 11 or 155 K/min (11 or 155 °C/min) was imposed under free-end or fixed-end conditions, *i.e.*, conditions that did not or did give rise to an axial stress/strain due to thermal contraction.

The effect of a prestrain in the beta phase field or concurrent straining along the RD of the sheet during cooling on variant selection was established in a second set of experiments. The former trials consisted of test conditions equivalent to those for the baseline experiments with the exception that a prestrain of 0.1 was imposed at an axial strain rate of 0.1 s^{-1} immediately prior to cooling. In the other set of experiments, deformation was imposed at a strain rate of the order of 10^{-5} or $3 \times 10^{-4} \text{ s}^{-1}$ during cooling at 11 or 155 K/min (11 or 155 °C/min), respectively. Because the load train was somewhat compliant, the strains developed by this means were between 0.02 and 0.05. Such conditions mirror the magnitude of (non-uniform) strains and strain rates that are developed in the interior of large titanium components during water quenching following beta annealing.

Following heat treatment, each sample was mounted, ground to the plan-view mid-plane, mechanically polished, and final electropolished prior to insertion into an XL30 field-emission-gun scanning electron microscope (FEI, Hillsboro, OR) for determination of the texture of the alpha phase. For this purpose, the microscope was operated at 20 kV and spot size 5 with a final aperture diameter of 100 μm , thereby producing a probe current of 49 nA. The stage was tilted 70 deg for all measurements. Local *alpha-phase* Kikuchi patterns produced as a result of electron-backscatter diffraction (EBSD) were collected over the entire sample face at a rate of ~ 210 frames per second using a step size of 8 μm (slow-cooled samples) or 4 μm (fast-cooled samples) and were analyzed with EDAX/TSL OIM™ software (EDAX Corp., Mahwah, NJ). The large scan area necessitated both beam and stage control and subsequent stitching of the resulting data.^[16,17]

Pole figures for the alpha phase were constructed from the EBSD data directly. Because of the limited volume fraction of the beta phase in Ti-6Al-4V at room temperature (~ 5 pct.), only limited EBSD results were obtained for this phase. Hence, an alternate method was applied to determine the orientations and hence texture of the underlying beta grains for the beta-annealed samples from the measurements for the alpha phase. This method was similar to that developed by Humbert *et al.*^[18,19] and Glavicic *et al.*^[20,21] For the present technique, however, the quaternion parameterization of orientation space was used in conjunction with average alpha-colony orientations (as described by Pilchak and Williams^[22]) in contrast to the pixel-by-pixel methods employed by the previous researchers. This enabled complete reconstruction of the beta grains in an area measuring $\sim 6 \text{ mm} \times 12 \text{ mm}$ (at full resolution) in several minutes. Typical beta grain

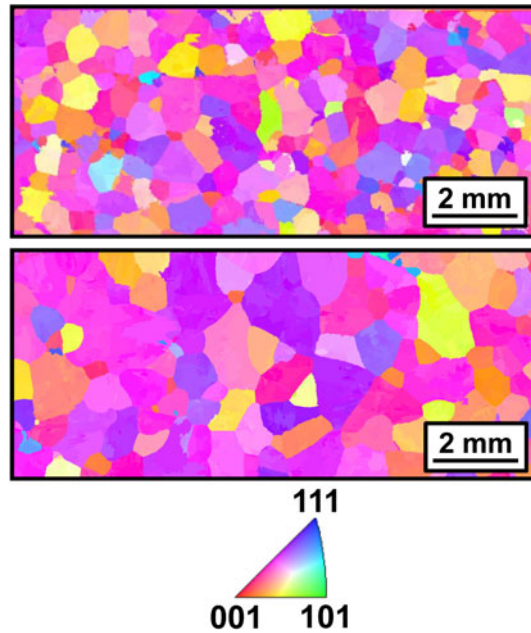


Fig. 3—Typical beta-grain microstructures which were reconstructed from EBSD-measured alpha-variant data for Ti-6Al-4V samples which were soaked 10 min above the transus and then cooled at 11 K/min (11 °C/min) under free-end conditions (top) or with concurrent deformation at an approximate strain rate of 10^{-5} s^{-1} (bottom).

structures reconstructed from the EBSD alpha-phase measurements are shown in Figure 3. Circle-equivalent beta-grain diameters and beta grain-size distributions (GSDs) for the beta-annealed samples were determined from the reconstructed beta grain structures using the EDAX/TSL OIM™ software. The average beta grain sizes so determined showed good agreement with those determined by applying the linear-intercept method to backscatter-electron micrographs. The average grain sizes and GSDs were typically based on at least 200 to 400 beta grains, except for a few coarse-grain cases involving ~ 100 to 150 grains.

Because the orientations of the alpha and beta phases in the as-received (alpha/beta processed) material did not follow the Burgers relation, the beta texture in this condition was determined from approximately 16,000 directly-measured beta-phase EBSD data points taken from an area identical in size to that used in the reconstruction method, *i.e.*, $\sim 6 \text{ mm} \times 12 \text{ mm}$, which was covered using a 2- μm step size.

Preferential variant selection was assessed by comparison of alpha-phase (0001) $_{\alpha}$ and beta-phase (110) $_{\beta}$ pole figures, whose intensity contours are reported in times-random units in all cases. Specifically, the degree of variant selection was quantified by determining the ratio R_{vs} of texture-component intensity maxima in the measured (0001) $_{\alpha}$ and reconstructed (011) $_{\beta}$ pole figures.

III. RESULTS AND DISCUSSION

The principal results of this investigation concerned the effect of process variables on the evolution of the

beta-phase texture during beta annealing and the subsequent evolution of alpha-phase textures and variant selection during cooling as affected by cooling rate and imposed stress or strain.

A. Evolution of Beta-Phase Microstructure and Texture

The beta microstructure and texture both showed a noticeable dependence on the process variables of soak time above the beta transus temperature and prestrain/concurrent strain during cooling. By and large, the average beta grain size developed in the baseline trials (*i.e.*, those that did not involve prestrain or concurrent strain during cooling) was approximately 220 or 390 μm for soak times of 0 or 10 minutes, respectively (Table I and Figure 4). The grain sizes for the short soak time (0 min) exhibited large scatter, however, perhaps due to the rapid growth at such times, sensitivity to specific test conditions, and/or the presence of alternating periods of slow and fast growth due to the texture-controlled-grain-growth effect.^[23,24] In particular, the sample that was held for 0 minutes and rapidly cooled exhibited the finest grain size (100 μm) most likely due to the limited time prior to transformation upon rapid cooling from the peak temperature. Despite such variations, the beta GSDs (*e.g.*, Figure 5) were similar in most cases with a ratio of largest-to-average beta grain diameter of approximately 3:1. The GSDs appeared to be log-normal for the finer beta grain sizes (Figure 5(a)). They were broadly similar for the larger beta sizes except that there was some scatter in the corresponding histograms (Figure 5(b)), perhaps because of the smaller number of grains that were sampled.

Despite the variability in the grain-size measurements, the degree of additional growth during the longer soak time was comparable to that predicted by a previous

phenomenological relation derived from short-time Ti-6Al-4V measurements,^[23] *i.e.*,

$$d^2 - d_0^2 = k(t - t_0)\exp(-Q/RT) \quad [1]$$

in which d and d_0 denote the instantaneous and initial beta grain sizes at times t and t_0 , respectively, the rate constant k equals 1110 m^2/s , Q is an apparent activation energy ($=312$ kJ/mol), and R is the gas constant. Calculations using Equation (1) revealed that an increase in grain size from 220 to 390 μm would require 450 seconds, or a time comparable to that utilized in the experiments, *viz.*, 600 seconds. Such agreement may be fortuitous, however, in view of the limited number of beta grains across the section of the 1500 μm -thick sheet samples and hence the propensity for grain growth to be two-, rather than three-, dimensional in nature.

Compared to the observations for the baseline trials, additional, strain-induced, beta grain growth was evident in the other experiments. In particular, samples which were subjected to a prestrain of 0.1 prior to cooling or concurrently deformed during cooling developed grain sizes approximately 50 to 100 pct larger than those developed in the baseline samples (Table I).

The beta textures developed during beta annealing revealed marked differences that appeared to depend primarily on soak time and thus grain growth (Figure 6). For example, samples that were soaked for 0 minutes upon reaching the peak temperature tended to show a noticeable TD component and other components (*e.g.*, an RD component) in $(011)_\beta$ pole figures, which were qualitatively similar to those in the as-received material (Figure 1(b)). These observations suggested that the beta grains grew from the small amount of this phase which was present in the as-received material, as previously found by Bhattacharyya *et al.*^[25] and Obasi *et al.*^[26] using in situ X-ray or neutron diffraction, respectively. However, the intensities of the

Table I. Beta Grain-Size Measurements

Sample ID	Soak Time (min)	Prestrain	Cooling Rate, K/min ($=^\circ\text{C}/\text{min}$)	Cooling Condition	Beta Grain Size (μm)	R_{vs}
12	0	0	11	free ends	310	1.7
14*	0	0	11	fixed ends	260	1.4
35	0	0	155	free ends	100	3.2
6	10	0	11	free ends	415	1.85
7	10	0	11	fixed ends	355	2.2
8	10	0	155	free ends	355	1.5
10	10	0	155	fixed ends	415	1.5
29	0	0.1	11	free ends	550	1.95
30*	0	0.1	11	fixed ends	575	2.0
38	10	0.1	11	free ends	950	2.25
27	10	0.1	11	fixed ends	700	2.8
26	10	0.1	155	free ends	655	1.8
28	10	0.1	155	fixed ends	660	1.5
31	10	0	11	$\dot{\epsilon} = 10^{-5} \text{ s}^{-1}$	775	2.15
32	10	0	11	$\dot{\epsilon} = 4 \times 10^{-5} \text{ s}^{-1}$	800	2.75
33*	10	0	155	$\dot{\epsilon} = 17.5 \times 10^{-5} \text{ s}^{-1}$	585	1.45
34	10	0	155	$\dot{\epsilon} = 70 \times 10^{-5} \text{ s}^{-1}$	795	1.35

*These conditions gave rise to a secondary $(0001)_z$ texture component of strength comparable to the primary component, but exhibited substantially lower values of R_{vs} .

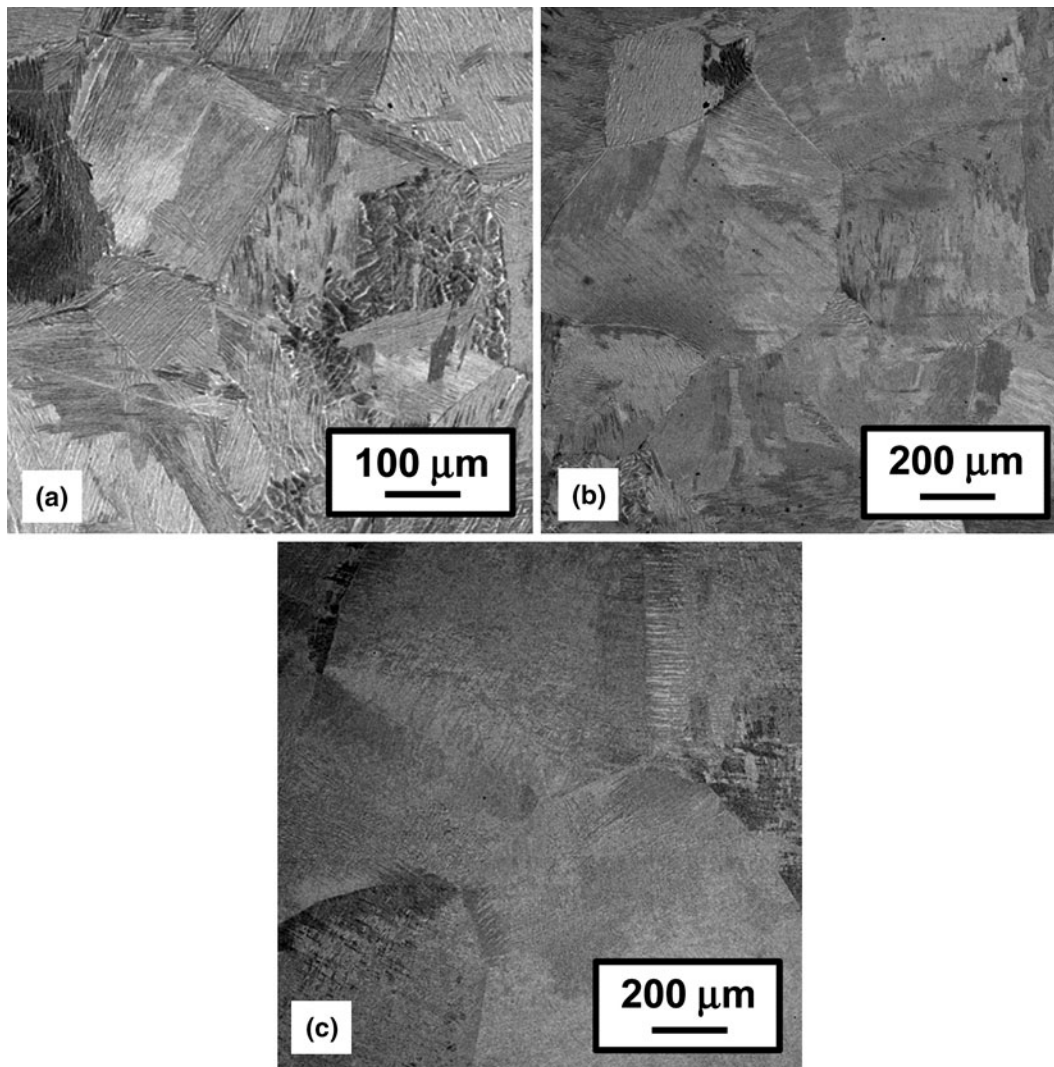


Fig. 4—Backscatter-electron images of typical microstructures developed in Ti-6Al-4V during beta annealing of (a) baseline sample soaked 0 min prior to cooling at 11 K/min (11 °C/min), (b) baseline sample soaked 10 min prior to cooling at 11 K/min (11 °C/min), and (c) sample soaked 10 min and concurrently strained while cooling at 155 K/min (155 °C/min).

various components in the heat-treated samples were weaker and somewhat different in relative magnitude in comparison to the initial condition. This latter effect can be ascribed to the evolution of texture associated with grain growth during the heating and cooling cycles for the 0-minute hold samples. As described by Ivasishin *et al.*^[24] in 2003, such texture-controlled grain growth may result in the strengthening of initially-weaker texture components and weakening of initially-stronger components. The conclusions of Ivasishin *et al.*^[24] on texture-controlled grain growth have also been recently corroborated by Obasi *et al.*^[26] using in situ neutron-diffraction measurements.

A 10-minute hold at the peak, beta-annealing temperature resulted in further evolution in the beta texture which can also be rationalized on the basis of texture-controlled grain growth. For this longer soak time, the RD component became the strongest, the TD was greatly reduced, and the split components lying between the ND and TD were maintained (Figure 6). Per the

Monte-Carlo grain-growth simulations in Reference 24, the observed changes in the intensity of the various principal texture components can give rise to alternating cycles of rapid and slow beta grain growth. Hence, the similarity of the degree of grain growth during the 10-minute soak period and prior measurements in Reference 23 may be fortuitous.

Evidence of texture-controlled grain growth was also found in other samples. Similar to the findings for baseline samples given a 10-minute soak prior to cooling, the beta textures of samples that were soaked for 10 minutes and concurrently strained during cooling tended to exhibit a predominant RD component, split components between the ND and RD of intermediate magnitude, and a weaker TD component in all cases except one (Figure 7).

Differences in the texture of the beta phase were also noted in orientation distribution functions (ODFs). The principal texture components lay along the so-called alpha fiber ($\phi_1 = 0$ deg, Φ , $\phi_2 = 45$ deg, in terms of

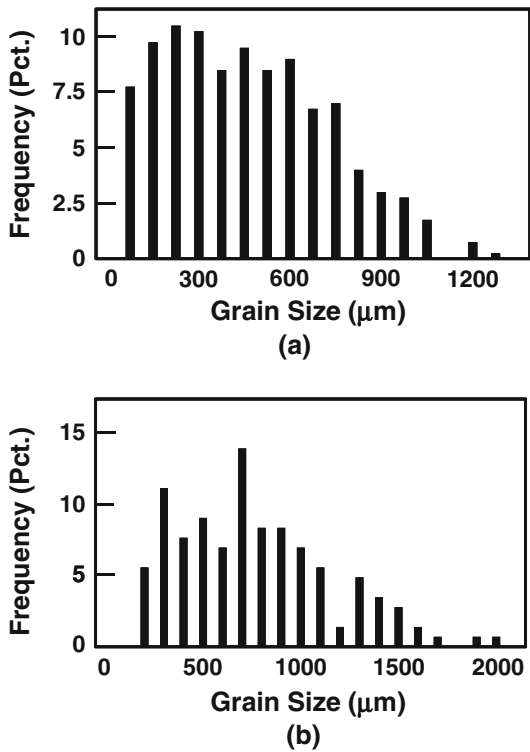


Fig. 5—Typical size distributions for reconstructed beta-grain microstructures of Ti-6Al-4V samples which were soaked 10 min above the transus and then cooled at 11 K/min (11°C/min) (a) under free-end conditions or (b) with concurrent deformation at an approximate strain rate of 10^{-5} s^{-1} .

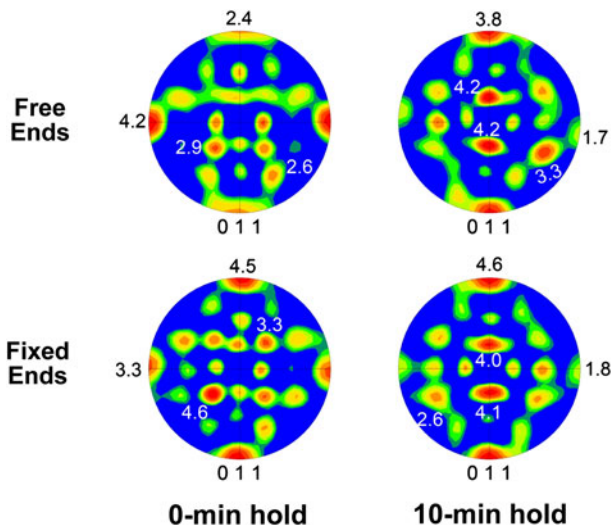


Fig. 6—Beta-phase $(011)_\beta$ pole figures reconstructed from measured alpha-phase EBSD measurements on Ti-6Al-4V samples which were beta annealed at peak temperature for 0 or 10 min followed by cooling at 11 K/min (11 °C/min) under free-end or fixed end conditions.

Bunge Euler angles). In particular, the beta texture of the as-received material and samples cooled with 0-minute soak time had a peak intensity at $\Phi \sim 0$ deg (Figure 8). Beta grain growth associated with a

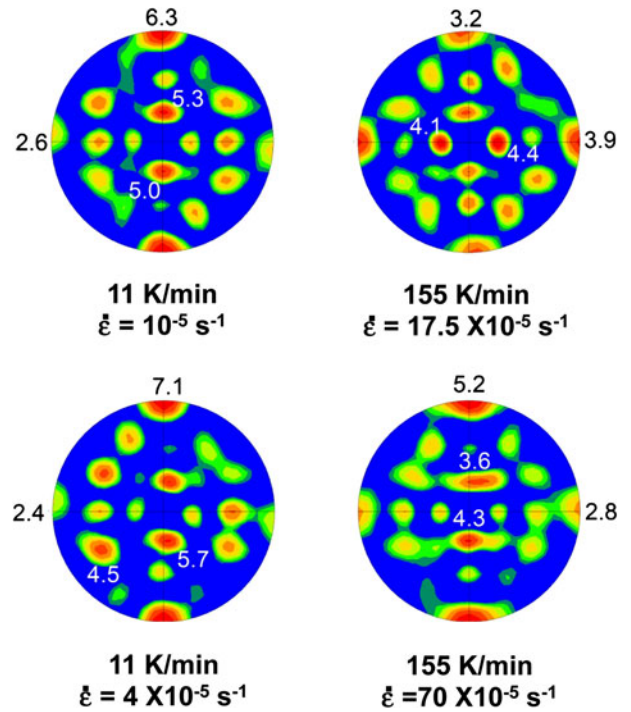


Fig. 7—Beta-phase $(011)_\beta$ pole figures reconstructed from measured alpha-phase EBSD measurements on Ti-6Al-4V samples which were beta annealed at peak temperature for 10 min and concurrently strained during cooling at the indicated rates.

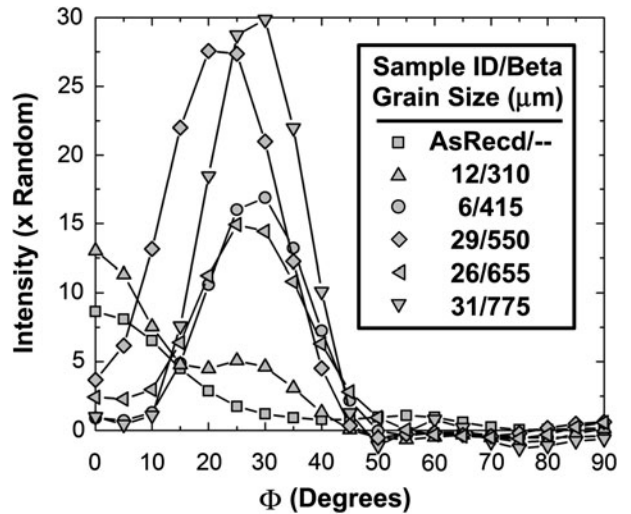


Fig. 8—Beta-phase texture intensity along the alpha fiber ($\phi_1 = 0$ deg, Φ , $\phi_2 = 45$ deg) for various samples in the present research program. See Table I for processing conditions associated with each sample ID.

10-minute soak and/or prestrain/concurrent straining tended to move the peak intensity to $\Phi \sim 25$ deg.

Despite the observed trends ascribed to texture-controlled grain growth, there were some differences in beta pole figures for each soak time. These differences were likely due to differences in initial texture at various locations in the as-received sheet and/or small variations in nominal test parameters. Because of these differences,

it was deemed critical that the magnitude of preferential variant selection, which is described in the following sections, be quantified in terms of the specific beta texture of each sample.

B. Variant Selection in Baseline Trials

For the baseline experiments, only a few conditions appeared to give rise to moderate-to-noticeable preferential variant selection as evidenced by a comparison of alpha-phase $(0001)_\alpha$ and beta-phase $(011)_\beta$ pole figures (Figures 9 and 10). The degree of variant-selection was assessed by determining the ratio R_{vs} of texture-component maxima in the measured $(0001)_\alpha$ and reconstructed $(011)_\beta$ pole figures. Not surprisingly, sample hypothetical calculations showed that the corresponding beta- and alpha-phase pole figures would be identical if the formation of all twelve alpha variants were equally probable (Figure 11), and R_{vs} would therefore equal unity. Thus, texture-component ratios greater than 1 served as quantitative measures of the degree of preferential variant selection.

For the *finer* beta grain size developed during 0-minute hold conditions and the slower cooling rate (11 K/min, or 11 °C/min), there appeared to be a modest degree of variant selection (Figure 9 and

Table I). The intensity of the principal texture component changed from 4.1 to $6.9\times$ random for the free-end case and from 4.4 to $6.2\times$ random for the fixed-end experiment. These values give moderate variant-selection ratios R_{vs} of 1.7 and 1.4, respectively. On the other hand, the sample which was cooled rapidly (155 K/min, or 155 °C/min) under free-end conditions and had the finest beta grain size observed in this research (*i.e.*, 100 μm) showed very strong beta- and alpha-phase textures and an R_{vs} of 3.2.

For the *coarser* beta grain size developed during the 10-minute hold, noticeable (preferential) variant selection was evident for the slower rate of cooling under both free-end and fixed-end conditions (Figure 10 and Table I). In both of these cases, strong RD alpha-phase texture components were formed. The values of R_{vs} were 1.85 (free ends) and 2.2 (fixed ends). By contrast, variant selection for the corresponding rapid-cooling cases was somewhat less. These conditions gave rise to R_{vs} values of approximately 1.5 in both instances, albeit the strongest component was still along the RD as for the coarse grain size, slow-cooled cases.

The observation of the relatively high degrees of preferential variant selection ($R_{vs} \sim 2$) for slow-cooled, *coarse-grain* material in the present work bears some similarity to the findings of Obasi *et al.*^[9] In this former

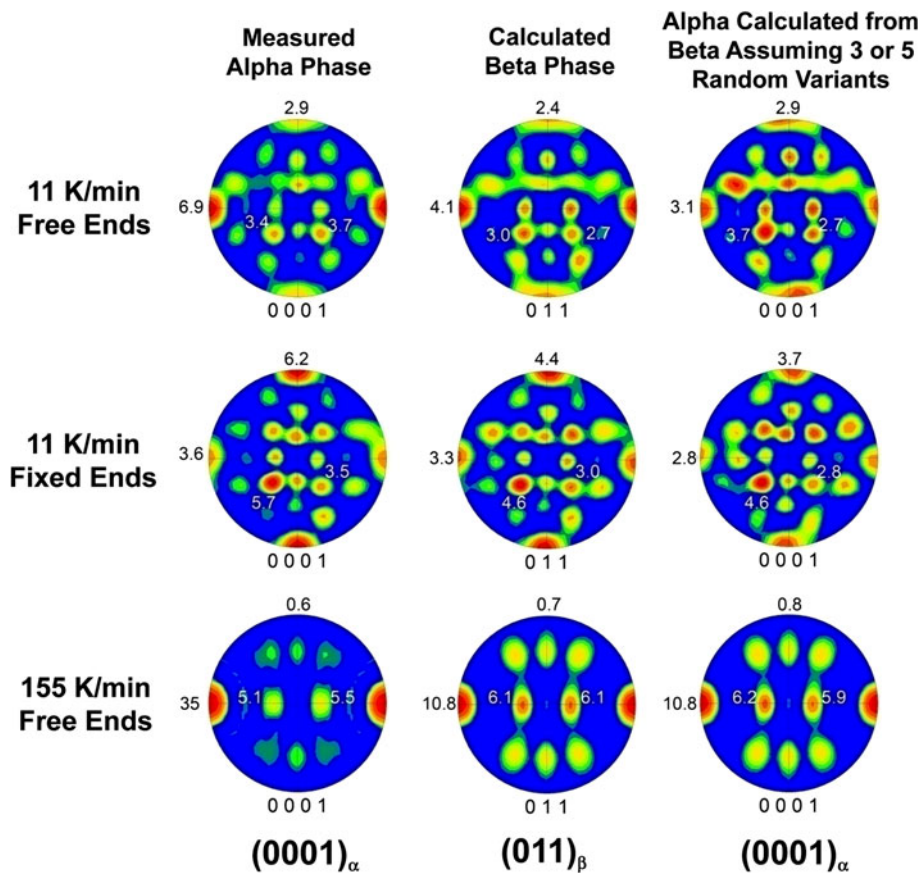


Fig. 9—Measured alpha-phase $(0001)_\alpha$ (left-hand column) and reconstructed beta-phase $(011)_\beta$, (center column) pole figures for baseline test samples soaked at peak temperature for 0 min and cooled at 11 or 155 K/min (11 or 155 °C/min) under free-end or fixed-end conditions. The right-hand column shows alpha pole figures calculated from the beta pole figures assuming the random selection of 3 variants (slow-cooled samples) or 5 variants (rapidly-cooled samples).

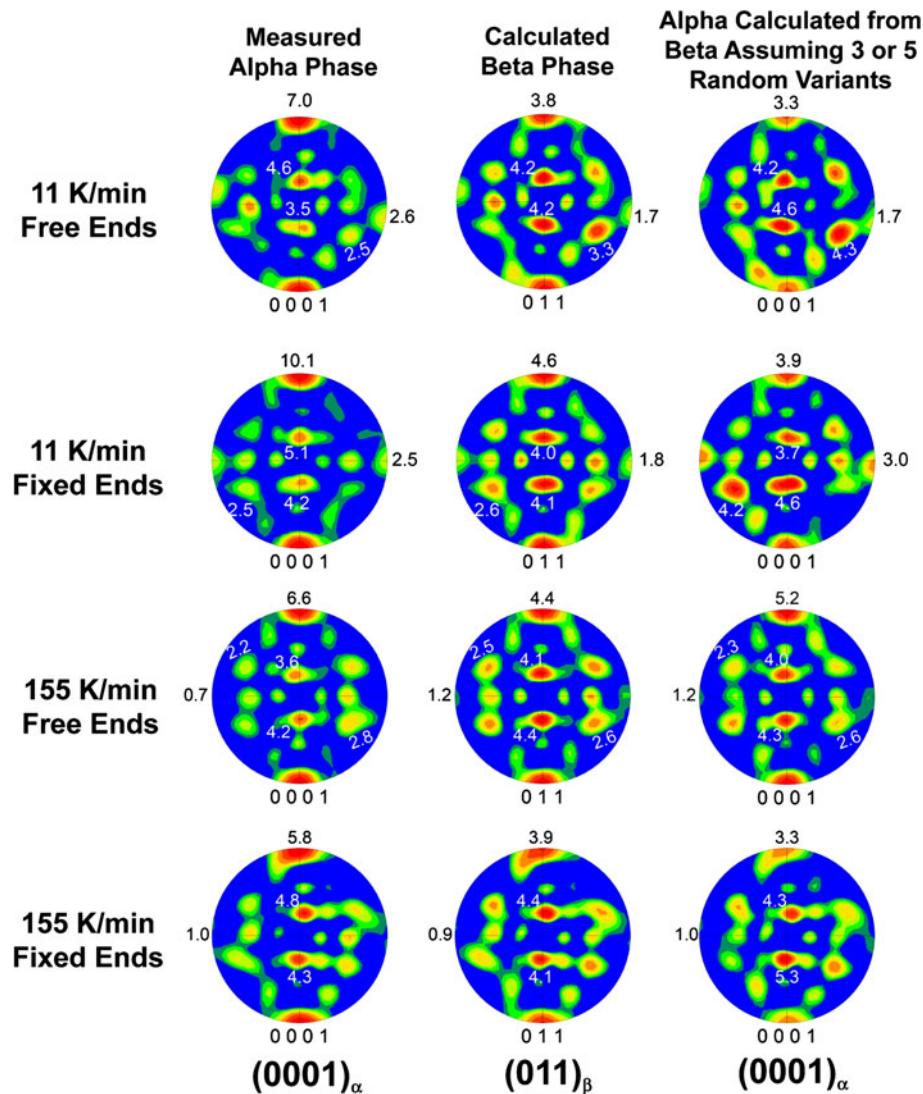


Fig. 10—Measured alpha-phase $(0001)_\alpha$ (left-hand column) and reconstructed beta-phase $(011)_\beta$ (center column) pole figures for baseline test samples soaked at peak temperature for 10 min and cooled at 11 or 155 K/min (11 or 155°C/min) under free-end or fixed-end conditions. The right-hand column shows alpha pole figures calculated from the beta pole figures assuming the random selection of 3 variants (slow-cooled samples) or 5 variants (rapidly-cooled samples).

research, preferred nucleation and relatively unimpeded growth due to a large beta grain size were surmised to be the source of the observed variant selection. However, the quantitative findings in the present work also revealed that (1) very strong variant selection ($R_{vs} \sim 3$) can be developed in very fine-grain material which is rapidly cooled and (2) a modest degree of variant selection ($R_{vs} \sim 1.5$) can occur for both slow-cooled, fine-grain and rapidly-cooled, coarse-grain samples. The latter results can be rationalized on the basis of limited growth of nucleated alpha variants in the slow-cooled samples due to the fine grain size or the development of a large chemical driving force (*i.e.*, supersaturation) developed under rapid-cooling conditions. A high supersaturation would be uniform throughout each beta grain and would thus tend to promote homogeneous and random, *intragranular* nucleation and growth of alpha variants.

The present results also revealed that imposed strains due to fixed-end conditions do not have a clear effect on variant selection in contrast to the findings of Gey *et al.*^[14] for substantially larger levels of strain. For the fine-grain, slow-cooled sample, the variant-selection ratio was *lower* for the fixed-end condition in comparison to that for free-end condition in which no strain was imposed. The reverse was true for the corresponding coarse-grain samples. These observations may be due to the very small axial strains associated with constrained thermal contraction in the present work, *i.e.*, ~ 0.015 to 0.02 . Such strains were large enough to produce noticeable surface roughening in comparison to the smooth surface which is retained from free-end experiments (Figure 12). However, it is important to realize that only a fraction of this very small strain was induced over the temperature regime in which substantial diffusional phase transformation occurs

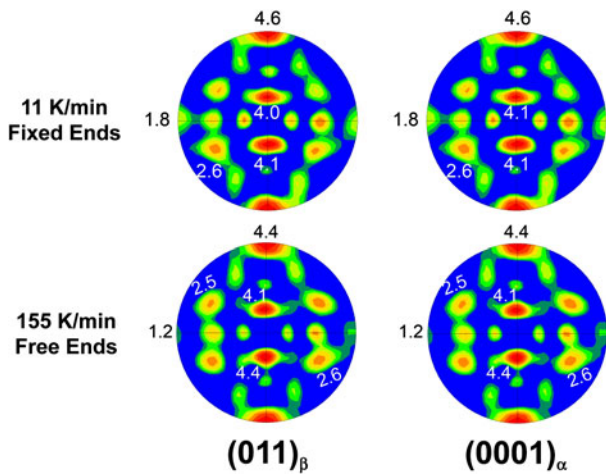


Fig. 11—Comparison of reconstructed beta-phase $(011)_\beta$ pole figures and alpha-phase $(0001)_\alpha$ pole figures calculated assuming all twelve possible variants form with equal probability for baseline samples which were cooled at 11 K/min (11 °C/min) under fixed-end conditions or 155 K/min (155 °C/min) under free-end conditions.

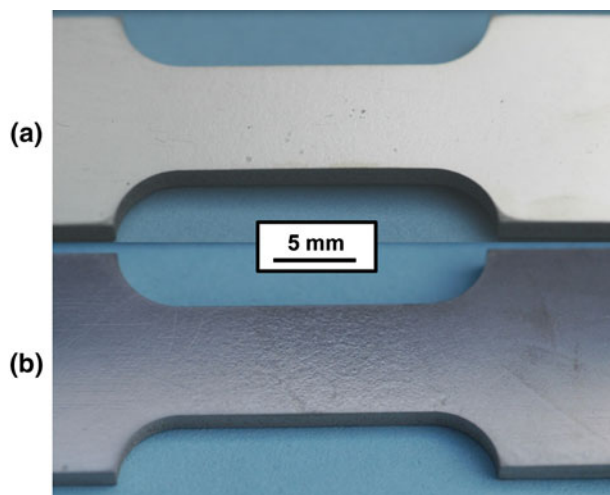


Fig. 12—Typical macrographs of Ti-6Al-4V sheet samples that were cooled under a (a) free-end or (b) fixed-end condition without a prestrain or concurrent straining.

(i.e., 1268 K \rightarrow 973 K, or \sim 995 °C \rightarrow 700 °C), although martensite (with $M_s \sim$ 963 K (690 °C) for Ti-6Al-4V^[27–29]) was not noticed in any of the samples.

C. Variant Selection in Trials Involving Prestrain or Concurrent Straining

The effect of cooling rate and deformation on variant selection during the baseline trials was further elucidated in the experiments involving a prestrain or concurrent straining. For example, a prestrain of 0.1 in the beta phase-field gave rise to noticeable preferential variant selection during slow cooling at 11 K/min (11 °C/min) for both grain sizes/soak times; non-random variant selection was more moderate for the samples which were rapidly-cooled at a rate of 155 K/min (155 °C/min) (Figures 13 and 14 and Table I). Specifically, the slow-cooled samples exhibited values of R_{vs} of approximately

2 (0-min soak, fine-grain samples) or 2.2 to 2.8 (10-min soak, coarse-grain samples). On the other hand, the rapidly cooled, coarse-grain samples exhibited R_{vs} values of 1.5 to 1.8. As for the baseline trials, the chemical driving force developed during rapid cooling likely mitigated the influence of prestrain and thus may have limited preferential variant selection. Nevertheless, each of the R_{sv} values was greater than that for the corresponding baseline trial involving no prestrain, irrespective of cooling rate.

The results in Figures 13 and 14 also revealed that, depending on the specific beta texture, alpha-phase textures which were strongest in the RD or TD were produced. For two of the six cases shown, a predominant RD $(0001)_\alpha$ component showed enhancement relative to the corresponding $(011)_\beta$ component. For the other four cases, a predominant TD component was enhanced. These results appear unusual in view of the work of Gey *et al.*^[14,15] in which the preferred variants were associated with highly-activated slip systems. For both the RD and TD texture components in the present work, the Schmid factors for tension along the RD and the two corresponding $\{110\}\langle 111\rangle$ slip systems were zero. (For the RD texture, the cosine of the angle between the tension axis and the slip-plane normal was zero. For the TD component, the cosine of the angle between the tension axis and each of the two possible slip directions within this slip plane was zero.) On the other hand, calculations for slip along $\{112\}\langle 111\rangle$ -type systems indicated that there were two with Schmid factors of 0.47. While the Burgers orientation relationship is commonly expressed in terms of (0001) and $\langle 2\bar{1}10\rangle$ in the alpha phase, crystallographic alignment also enforces one set of $\{10\bar{1}0\}_\alpha$ and $\{112\}_\beta$ planes to be parallel. These planes correspond to the terraces on the broad face of the alpha lath and contain c-type misfit dislocations. The specific $\{110\}$ plane associated with the high Schmid factor $\{112\}\langle 111\rangle$ slip systems were both aligned with the TD direction, indicating that dislocation activity may have contributed to the strengthened TD texture component for cases involving a prestrain. It is noteworthy, however, that the TD component was not enhanced for all cases (Figures 13 and 14), and thus other mechanisms may have also been important in the present case.

The observations for experiments involving deformation imposed concurrent with cooling were similar to those in which samples were prestrained prior to cooling. In other words, straining during slow or rapid cooling led to noticeable or modest preferential variant selection, respectively (Figure 15 and Table I). For both strain rates that were used, the RD texture component in the high-temperature beta phase $(011)_\beta$ pole figure gave rise to a stronger RD component in the corresponding alpha-phase $(0001)_\alpha$ pole figure. The values of R_{vs} were 2.15 and 2.75 for the two experiments for the slower cooling rate and 1.45 and 1.35 for those using the faster cooling rate. Again, these findings contrast with those summarized in Gey *et al.*^[14,15] with regard to the specific texture component which was enhanced. However, the levels of deformation imposed on the present concurrently-strained samples over the transformation

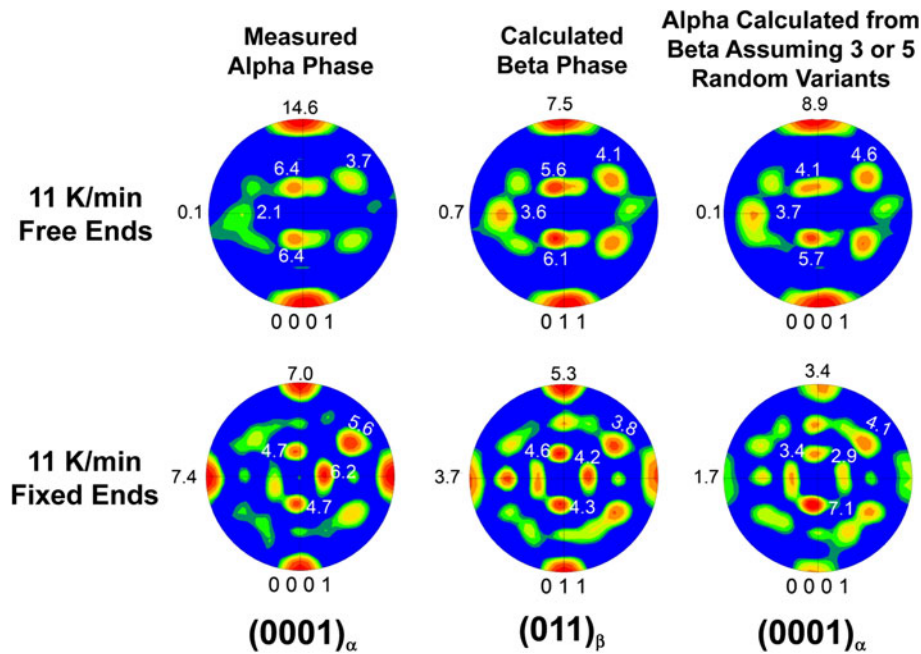


Fig. 13—Measured alpha-phase $(0001)_\alpha$ (left-hand column) and reconstructed beta-phase $(011)_\beta$, (center column) pole figures for test samples soaked at peak temperature for 0 min, deformed to a prestrain of 0.1, and cooled at 11 K/min (11 °C/min) under free-end or fixed-end conditions. The right-hand column shows alpha pole figures calculated from the beta pole figures assuming the random selection of 3 variants (slow-cooled samples) or 5 variants (rapidly-cooled samples).

temperature interval (after correction for test machine compliance) were ~ 0.02 – 0.06 , or values considerably smaller than those in the research of Gey *et al.*

D. Interpretation of Variant-Selection Observations

As noted in Section III–B, random variant selection involving all twelve possible variants would give rise to $(0001)_\alpha$ pole figures essentially identical to the corresponding $(011)_\beta$ pole figures. The observations showed that this was not the case. Hence, insight into the mechanism of variant selection was sought from a number of supplemental numerical simulations which are described in this section.

The first set of calculations was based on the common observation that beta-phase decomposition usually gives rise to the apparent predominance of a small subset of the twelve possible variants, the exact number increasing with increasing cooling rate. Therefore, simulations of the evolution of alpha-phase textures were conducted assuming the random selection of 3 or 5 variants for the slow or fast cooling-rate cases, respectively. The $(0001)_\alpha$ textures so predicted (third column in Figures 9, 10, 13 through 15) showed generally poor agreement with the measurements (first column in Figures 9, 10, 13 through 15).

Second, numerical calculations were performed to establish the applicability of two criteria which have been used in the past to interpret variant selection for alpha/beta titanium alloys, *viz.*: (1) The presence (or absence) of parallel (or nearly parallel) $\{011\}_\beta$ -type planes in adjacent beta grains which enhances variant nucleation and promotes the growth of a specific variant

across the grain boundary^[10] and (2) the minimization of the elastic strain energy associated with the $\beta \rightarrow \alpha$ phase transformation.^[30]

To test the first criterion, the probability of the occurrence of beta grain pairs/boundaries having nearly-parallel $\{110\}$ planes within various tolerance angles was calculated for three of the beta textures in the present work. For each example, pairs of Euler angles were selected at random from the list of discrete orientations representing the specific texture. The angles between all $\{110\}$ planes in the two orientations were calculated. The resulting plots of probability as a function of (tolerance) angle showed qualitatively-similar behavior for the three cases investigated (Figure 16). However, the beta texture which exhibited the highest probability for a given tolerance angle (sample 14) had a relatively modest value of R_{sv} (1.4). The apparent lack of correlation between the degree of preferential selection and the high probabilities for this case can be rationalized on the basis of fine beta grain size due to a short soak time. By contrast, for sample 7 for which R_{sv} was 2.2, the probabilities for near-common $\{110\}_\beta$ planes were relatively low. Hence, further research is deemed appropriate to evaluate further the criterion suggested by Bhattacharyya *et al.*^[10]

For the second criterion, alpha-phase texture predictions were made based on choosing the 3 or 5 variants for the slow-cooled or rapidly-cooled samples, respectively, with the lowest strain energy for each beta grain in a given beta-texture file. For this purpose, the energy was calculated as the tensor product of the stress state (assumed as a first approximation to be simply an uniaxial tensile stress for all grains) and the strain associated with the beta-to-alpha transformation for

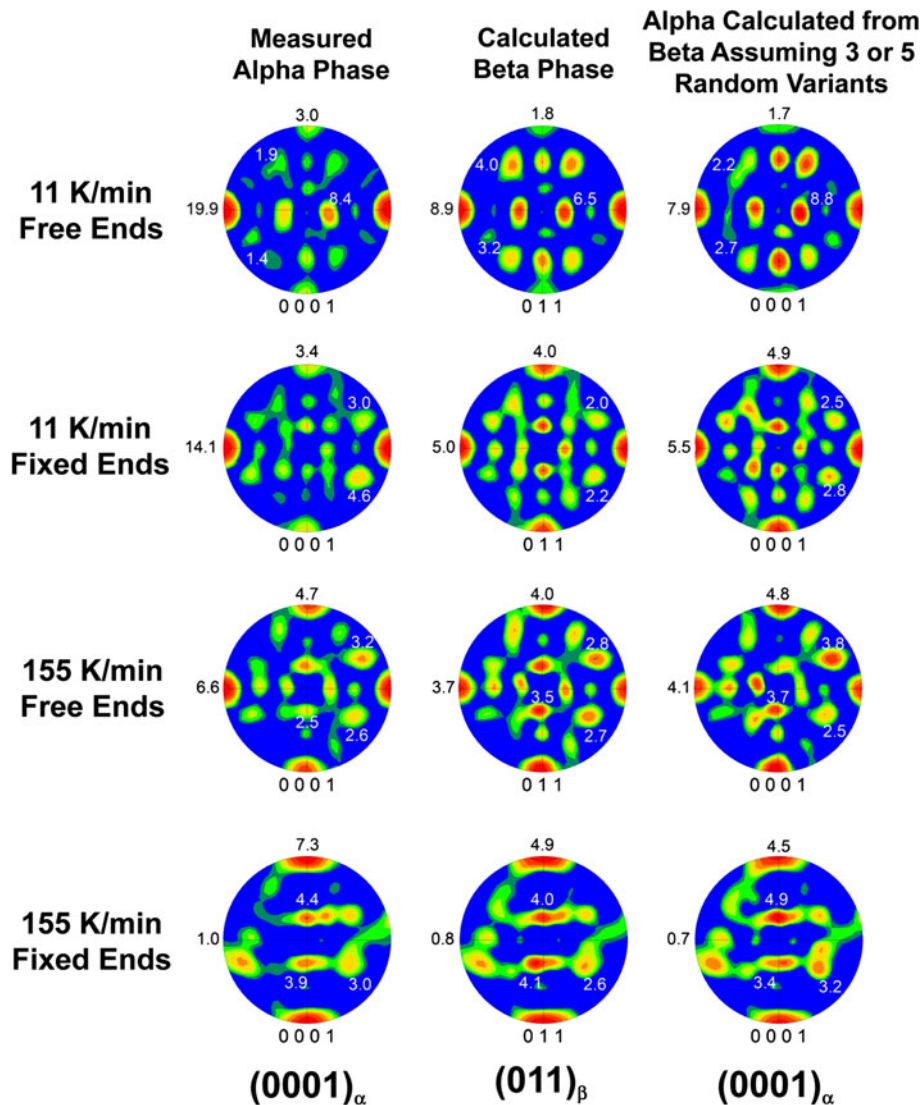


Fig. 14—Measured alpha-phase $(0001)_\alpha$ (left-hand column) and reconstructed beta-phase $(011)_\beta$ (center column) pole figures for test samples soaked at peak temperature for 10 min, deformed to a prestrain of 0.1, and cooled at 11 or 155 K/min (11 or 155 °C/min) under free-end or fixed-end conditions. The right-hand column shows alpha pole figures calculated from the beta pole figures assuming the random selection of 3 variants (slow-cooled samples) or 5 variants (rapidly-cooled samples).

each of the twelve possible variants (tensor transformed into the sample coordinate system).^[31] The results for the two baseline, coarse-grain, fixed-end cases are shown in Figure 17. Unfortunately, these predicted textures showed major differences with the corresponding measurements (Figure 10).

The apparent lack of agreement between the measurements and predictions based on a strain-energy model may be a result partly of the Sachs isostress assumption; *i.e.*, the stress state in each grain was likely much more complicated and non-uniform. On the other hand, the nature of the sheet-sample geometry used in the present work and the beta textures developed prior to transformation per se may provide an alternate means of rationalizing the observations. In particular, the grain sizes developed during beta annealing were of the order of 200 to 400 μm for the baseline samples and

even larger in the prestrained or concurrently-strained samples. Thus, there were relatively few grains across the section, especially for the coarser microstructures. Second, the principal component of the beta textures comprised a 011 plane normal to the RD or TD with the rolling plane being close to a 100 direction. As described in References 32 and 33, the distortion associated with the transformation of beta to alpha consists primarily of a contraction along a 011 direction and an extension along a 100 direction in the beta crystals. For a sheet specimen with the types of beta textures in the present work, it may therefore be hypothesized that the required shape change would be relatively easy when the extension strain occurred in the thickness direction because of the limited through-thickness constraint associated with the thinness of the sample and limited number of surrounding beta grains in this direction.

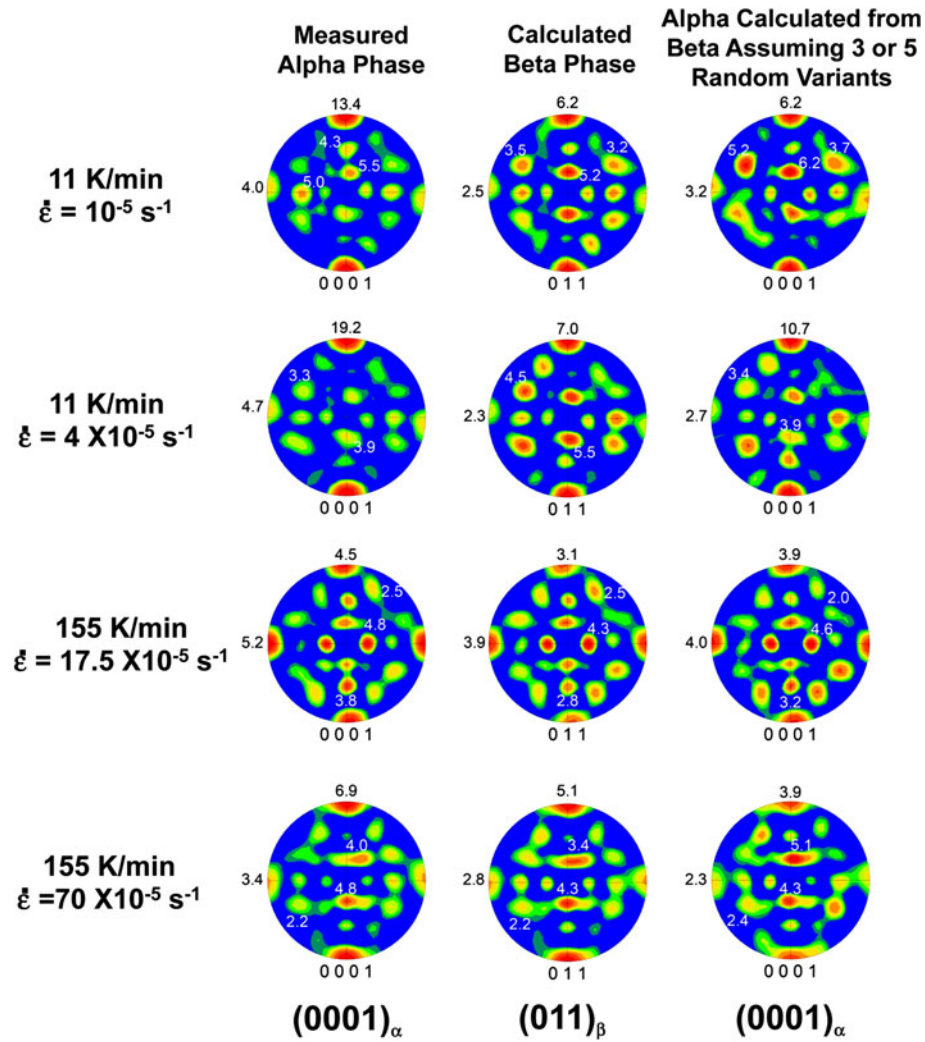


Fig. 15—Measured alpha-phase $(0001)_\alpha$ (left-hand column) and reconstructed beta-phase $(011)_\beta$, (center column) pole figures for test samples soaked at peak temperature for 10 min and concurrently cooled and strained at the rates indicated. The right-hand column shows alpha pole figures calculated from the beta pole figures assuming the random selection of 3 variants (slow-cooled samples) or 5 variants (rapidly-cooled samples).

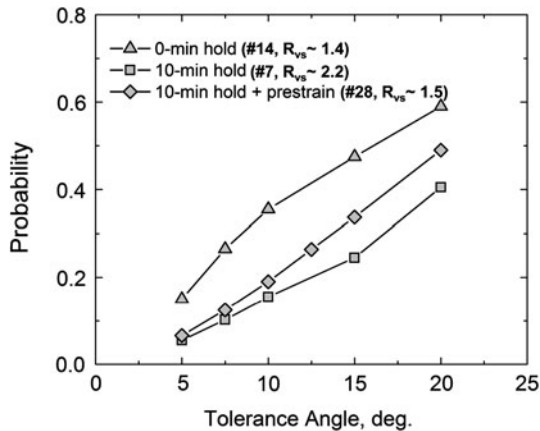


Fig. 16—Probability of having a common 110-plane across beta grain boundaries as a function of tolerance angle for the beta textures of samples which were soaked 0 min and then cooled at 11 K/min (11 °C/min) under fixed-end conditions (triangles), soaked 10 min and then cooled at 11 K/min (11 °C/min) under fixed-end conditions (squares), or soaked 10 min, prestrained 0.1, and cooled at 155 K/min (155 °C/min) under fixed-end conditions (diamonds).

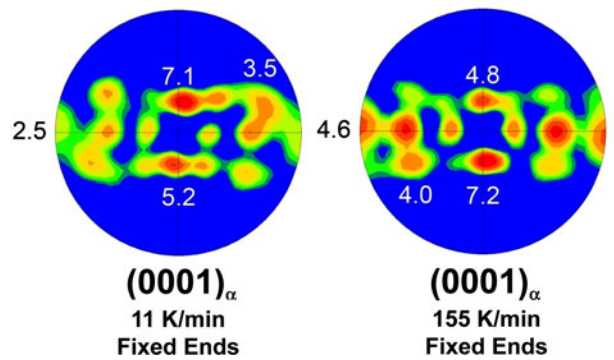


Fig. 17—Predicted alpha-phase $(0001)_\alpha$ pole figures based on a minimum-strain-energy variant-selection criterion for baseline samples soaked at peak temperature for 10 min and then cooled at 11 or 155 K/min (11 or 155 °C/min) under fixed-end conditions.

IV. SUMMARY AND CONCLUSIONS

The effect of process variables on preferential variant selection following beta annealing of a typical alpha/beta sheet titanium alloy was determined. From this work, the following conclusions were drawn:

1. The texture of the beta phase may change noticeably during beta annealing as a result of grain growth. Hence, preferential (non-random) variant selection must be interpreted in terms of the specific beta-phase texture immediately prior to decomposition.
2. Preferential variant selection tends to occur more readily under moderately slow cooling conditions (e.g., ~ 10 K/min, or ~ 10 °C/min) following beta annealing. The development of a coarse beta grain size during beta annealing or the application of strains of the order of approximately 0.02 to 0.10 prior to or concurrently with cooling tends to increase the degree of preferential variant selection. Small strains developed due to constrained thermal contraction lead to a lower degree of preferential variant selection. The only exception to these trends appears to be for samples with very fine beta grain size (~ 100 μm) which are cooled rapidly from the beta phase field.
3. The variants which are selected in cases involving the application of modest strains (~ 0.02 to 0.10) prior to or during cooling from the beta phase field do not necessarily appear to correlate with those beta-phase slip systems which have been most highly activated.
4. Preferential variant selection during rapid cooling (at ~ 150 K/min, or ~ 150 °C/min) is considerably less than during slow cooling, most likely due to the large and uniform chemical driving force associated with the development of a high supersaturation which tends to promote homogeneous nucleation of alpha variants within each beta grain.
5. Variant selection rules such as that based on near-parallel $\{110\}$ planes in adjacent beta grains appear to provide a qualitative, but not quantitative, explanation of observations of variant selection. On the other hand, the present observations may be rationalized on the basis of the limited through-thickness constraints associated with the type of sample that was used and the small number of grains across the section.
6. The complexity of the effects of starting texture, product form (e.g., sheet versus forging), and process variables on variant selection suggests that additional work is needed to understand this complex phenomenon more fully.

ACKNOWLEDGMENTS

This work was conducted as part of the in-house research of the Metals Branch of the Air Force Research Laboratory's Materials and Manufacturing Directorate.

The support and encouragement of the Laboratory management is gratefully acknowledged. Two of the authors were supported under Air Force contracts FA8650-09-2-5800 (KTK) and FA8650-04-D-5235 (GAS). Technical discussions with M.G. Glavicic (Rolls-Royce, Indianapolis, IN) and A.A. Salem (Materials Resources, LLC) are greatly appreciated.

REFERENCES

1. D. Dunst and H. Mecking: *Zeitschrift für Metallkunde*, 1996, vol. 87, pp. 498–507.
2. N.R. Barton and P.R. Dawson: *Model. Simul. Mater. Sci. Eng.*, 2001, vol. 9, pp. 433–63.
3. S.V. Divinski, V.N. Dnieprenko, and O.M. Ivasishin: *Mater. Sci. Eng. A*, 1998, vol. A243, pp. 201–05.
4. M. Humbert, L. Germaine, N. Gey, P. Bocher, and M. Jahazi: *Mater. Sci. Eng. A*, 2006, vol. A430, pp. 157–64.
5. L. Zeng and T.R. Bieler: *Mater. Sci. Eng. A*, 2005, vol. A392, pp. 403–14.
6. W.G. Burgers: *Physica*, 1934, vol. 1, pp. 561–86.
7. D. He, J.C. Zhu, S. Zaefferer, D. Raabe, Y. Liu, Z.L. Lai, and X.W. Yang: *Mater. Sci. Eng. A*, 2012, vol. A549, pp. 20–29.
8. N. Stanford and P.S. Bate: *Acta Mater.*, 2004, vol. 52, pp. 5215–24.
9. G.C. Obasi, S. Biroscas, J. Quinta da Fonseca, and M. Preuss: *Acta Mater.*, 2012, vol. 60, pp. 1048–58.
10. D. Bhattacharyya, G.B. Viswanathan, R. Denkenberger, D. Furrer, and H.L. Fraser: *Acta Mater.*, 2003, vol. 51, pp. 4679–91.
11. G.C. Obasi, S. Biroscas, D.G.L. Prakash, J. Quinta da Fonseca, and M. Preuss: *Acta Mater.*, 2012, vol. 60, pp. 6013–24.
12. S.L. Semiatin, P.N. Fagin, M.G. Glavicic, I.M. Sukonnik, and O.M. Ivasishin: *Mater. Sci. Eng. A*, 2001, vol. A299, pp. 225–34.
13. H. Moustahfid, N. Gey, M. Humbert, and M.J. Philippe: *Metall. Mater. Trans. A*, 1997, vol. 28A, pp. 51–59.
14. N. Gey, M. Humbert, M.J. Philippe, and Y. Combres: *Mater. Sci. Eng. A*, 1996, vol. A219, pp. 80–88.
15. N. Gey, M. Humbert, M.J. Philippe, and Y. Combres: *Mater. Sci. Eng. A*, 1997, vol. A230, pp. 68–74.
16. A.R. Shively, P.A. Shade, A.L. Pilchak, J.S. Tiley, and R. Kerns: *J. Microsc.*, 2011, vol. 244, pp. 181–86.
17. A.L. Pilchak, A.R. Shively, J.S. Tiley, and D.L. Ballard: *J. Microsc.*, 2011, vol. 244, pp. 38–44.
18. M. Humbert, H. Moustahfid, F. Wagner, and M.J. Philippe: *Mater. Sci. Forum*, 1994, vol. 157, pp. 1225–30.
19. M. Humbert, F. Wagner, H. Moustahfid, and C. Esling: *J. Appl. Cryst.*, 1995, vol. 28, pp. 571–76.
20. M.G. Glavicic, P.A. Kobryn, T.R. Bieler, and S.L. Semiatin: *Mater. Sci. Eng. A*, 2003, vol. A346, pp. 50–59.
21. M.G. Glavicic, P.A. Kobryn, T.R. Bieler, and S.L. Semiatin: *Mater. Sci. Eng. A*, 2003, vol. A351, pp. 258–64.
22. A.L. Pilchak and J.C. Williams: *Metall. Mater. Trans. A*, 2011, vol. 42A, pp. 773–94.
23. S.L. Semiatin, J.C. Soper, and I.M. Sukonnik: *Acta Mater.*, 1996, vol. 44, pp. 1979–86.
24. O.M. Ivasishin, S.V. Shevchenko, N.L. Vasiliev, and S.L. Semiatin: *Acta Mater.*, 2003, vol. 51, pp. 1019–34.
25. D. Bhattacharyya, G.B. Viswanathan, S.C. Vogel, D.J. Williams, V. Venkatesh, and H.L. Fraser: *Acta Mater.*, 2006, vol. 54, pp. 231–36.
26. G.C. Obasi, R.J. Moat, D.G.L. Prakash, W. Kockelmann, J. Quinta da Fonseca, and M. Preuss: *Acta Mater.*, 2012, vol. 60, pp. 7169–82.
27. H.J. Hucek: *Aerospace Structural Metals Handbook*. Metals and Ceramics Information Center, Battelle, Columbus, OH, 1991.
28. V.N. Gridnev, O.M. Ivasishin, and S.P. Oshkaderov: in *Titanium, Science and Technology*, G. Lütjering, U. Zwicker, and W. Bunk, eds., Deutsche Gesellschaft für Metallkunde e.V., Oberursel, 1985, pp. 1635–41.
29. E.W. Collings: *The Physical Metallurgy of Titanium Alloys*, ASM, Materials Park, OH, 1984, ch. 4.

30. C. Shen, J.P. Simmons, and Y. Wang: *Acta Mater.*, 2006, vol. 54, pp. 5617–30.
31. G.A. Sargent, K.T. Kinsel, A.L. Pilchak, A.A. Salem, and S.L. Semiatin: *Metall. Mater. Trans. A*, 2012, vol. 43A, pp. 3570–85.
32. M. Humbert, L. Germaine, N. Gey, P. Bocher, and M. Jahazi: *Mater. Sci. Eng. A*, 2006, vol. 430, pp. 157–64.
33. A. Kelly, G.W. Groves, and P. Kidd: *Crystallography and Crystal Defects*, Wiley, West Sussex, 2000.